analytical chemistry

pubs.acs.org/ac Article

Capping Ligand Size-Dependent LSPR Property Based on DNA Nanostructure-Mediated Morphological Evolution of Gold Nanorods for Ultrasensitive Visualization of Target DNA

Meng-Qi He, Shuai Chen, Jie Meng, Wei Shi, Kun Wang, Yong-Liang Yu,* and Jian-Hua Wang*

Cite This: *Anal. Chem.* 2020, 92, 7054−7061 Read Online

ACCESS | Metrics & More | Article Recommendations | Supporting Information

ABSTRACT: Systematically tuning the structures and properties of noble-metal nanoparticles through biomolecule-mediated overgrowth is of significant importance for their applications in biosensing and imaging. Herein thiolated biomolecules with different concentrations and sizes (molecular weight and spatial structure) were used as a class of capping ligands to control the longitudinal surface plasmon resonance (LSPR) property of gold nanorods (GNRs). The LSPR peaks were red-shifted by increasing the capping agent concentration. The size effect could be divided to two aspects: (1) When the ligands are small molecules, the LSPR peak is blue-shifted as the size of the capping ligand increases. (2) When the ligands are macromolecular proteins, the LSPR property is similar to that of the overgrown nanoparticle (Au@gap@GNR) without thiolated biomolecules as capping agents. Interestingly, thiol-free and nonhomooligomeric DNA strands as capping agents present a similar influence in shaping the overgrowth of GNRs by varying their concentrations and sizes. In addition, the size effect of a DNA nanostructure was used to construct a $\Delta\lambda_{LSPR}$-based catalytic nucleic acid biosensor using a DNA dendritic nanostructure as a capping agent combined with LSPR signals generated from the Au@gap@GNRs with morphological evolution. More importantly, the $\Delta\lambda_{LSPR}$-based biosensor possesses three advantages in nucleic acid biosensing: (1) It is completely label- and wash-free, (2) it has an ultrahigh sensitivity and signal-to-noise ratio, and (3) it can be visualized without any instrumental aid, indicating a significant potential for ultrasensitive biosensing.

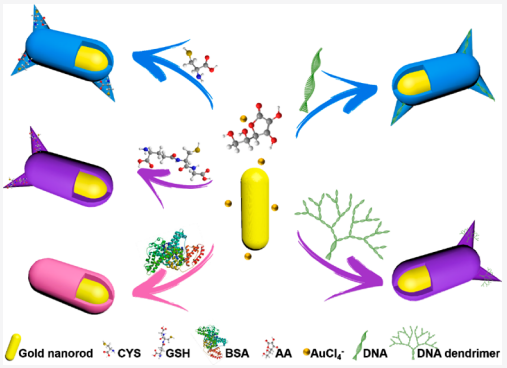

INTRODUCTION

Seed-mediated overgrowth of noble-metal nanoparticles using functional capping ligands is a versatile and effective approach to controlling the physical and chemical properties of nanoparticles for various applications ranging from catalysis to biosensing, imaging, electronics, and photonics.[1−3] One of the most specific properties of the overgrown nanoparticles is the longitudinal surface plasmon resonance (LSPR), which is a unique optical property of anisotropic noble-metal nanoparticles (such as gold nanorods (GNRs)) that can be tuned by the morphological evolution of the nanoparticle.[4−6] The most general method to regulate the LSPR property is employing different kinds of capping ligands that favor specific facets of the nanoparticles in the overgrowth of GNRs.[7−9] For example, compared with the hexadecyltrimethylammonium bromide (CTAB)−Au interactions on the (100) and (110) side faces, CTAB−Au interactions on the (111) end faces have a lower binding affinity, resulting in the preferential binding of thiolated biomolecules to the end faces through the formation of strong Au−S bonds.[10−12] However, the effect of the inherent concentration and size of molecular ligands on the morphological evolution and LSPR property of GNRs has been rarely studied. Notably, amino acids (L-cysteine (CYS)), peptides (L-glutathione (GSH)), proteins (bovine serum albumin (BSA)), and other thiolated biomolecules, which are different in size, act in different manners in shaping in the overgrowth of GNRs as capping agents.[13,14]

To fully investigate the mechanism of GNR overgrowth using capping ligands with different sizes, DNA molecules as a class of capping ligands were used to control the morphological and optical properties of GNRs.[15,16] Because of their unique programmable and functional ability following the highly specific Watson−Crick base-pairing rule, DNA sequences can form various geometries and motifs and can even precisely assemble into DNA nanostructures (1D, 2D, and 3D structures) of different sizes.[17−19] In addition, because of their varying charge, length, affinity, and functional groups, DNA molecules as capping agents show extra capability for precisely tuning the properties of the overgrowth of GNRs as

Received: January 21, 2020
Accepted: April 27, 2020
Published: April 27, 2020

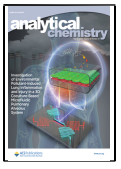

https://dx.doi.org/10.1021/acs.analchem.0c00321
Anal. Chem. 2020, 92, 7054−7061

Scheme 1. (A) Synthesis of Au@gap@GNRs via Seed-Mediated Growth Using Different Sizes of Thiolated Molecules or a DNA/DNA Dendrimer Nanostructure and (B) Components and Reaction Pathway of the DNA Dendrimers

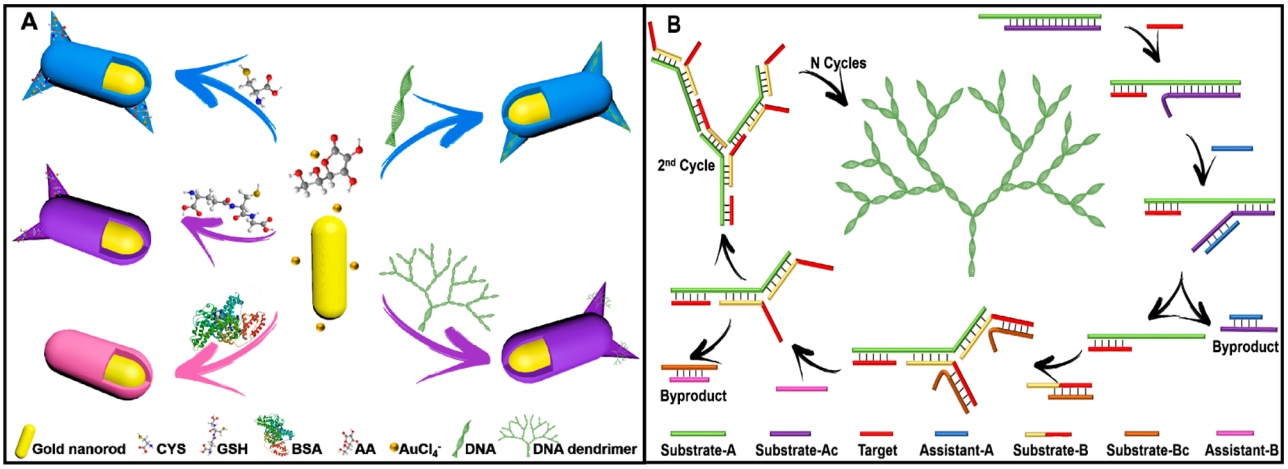

thiolated molecules.[20] Recently, homooligomeric DNA molecules have been used as the capping agents to control the morphologies and LSPR properties of GNRs due to the different binding affinities between DNA nucleobases and nanoparticles.[21] However, the sequence-dependent "DNA-encoded" overgrowth of nanoparticles limits the application of DNA nanotechnology in combination with optical signals generated by the morphological evolution of nanoparticles.[22,23] For example, sequence-dependent DNA cannot form DNA nanostructures with different sizes and shapes as capping agents to control the morphologies and LSPR properties of the overgrown nanoparticles. Therefore, nonhomooligomeric DNA molecules, as capping ligands and modules of DNA nanotechnology in the overgrowth of GNRs, are of great value for exploring the synthetic mechanisms and applications of the generated overgrown nanoparticles with tunable geometric and plasmonic properties.

Surface plasmon resonance (SPR) intensity-based absorption analysis is not reliable considering the broad Vis−NIR spectra among the variation in SPR peak positions.[24,25] It is also difficult to achieve complete quenching using switch-based fluorescence analysis, which also increases the background.[26,27] Fortunately, LSPR peak-shift-based biosensors possess unique advantages in sensing and detecting biomolecules due to their ultrahigh sensitivity and signal-to-noise ratio.[28,29] Recently, LSPR peak shifts as detection signals have generally been regulated by assembling nanoparticles, which require a specific surface modification of GNRs under extremely harsh experimental conditions.[30] In addition, the stability of the LSPR property is a critical issue because the aggregation and disassembly of GNRs cause the variation and even the disappearance of signals.[31] To solve the stability issues, a few strategies were used to precisely tune the LSPR property by controlling the morphologies of overgrown nanoparticles.[32,33] One of the methods is the seed-mediated overgrowth of noble-metal nanoparticles using functional capping ligands.

In this work, thiolated biomolecules (such as CYS, GSH, and BSA) with different concentrations and sizes were used as capping ligands to shape the morphologies and the LSPR property of GNRs (Scheme 1A). The tuning mechanisms of the LSPR property, depending on the capping ligand, were also investigated. It was found that the red shift of the LSPR peak was achieved by increasing the concentration of the capping agent; the size effect of the capping agent can be divided into two situations: When the ligands are small molecules, the LSPR peak is blue-shifted and the color of the solution changes from blue to purple with the increase in the size of capping agent under the same concentration; when the ligands are macromolecular proteins, the size of the capping ligands is too large to be wrapped, resulting in morphologies and LSPR properties similar to the overgrown nanoparticles (Au@gap@GNRs) without capping agents. Interestingly, we have shown that thiol-free and nonhomooligomeric DNA strands have a similar influence in the overgrowth of GNRs. In understanding the mechanism of the concentration effect from DNA strands, two observations were noted in the overgrowth: (1) The red shift of the LSPR peak is independent of the DNA nucleobases, except for T, and (2) the transverse surface plasmon resonance (TSPR) peak is dependent on the DNA nucleobases, except for T. DNA molecules are excellent material modules for assembling nanostructures with different sizes, providing spatial and dynamic control due to their programmability and predictable base−pair interactions. DNA nanostructures with different sizes act as capping agents in the overgrowth of GNRs, extending the application of DNA nanotechnology in combination with the LSPR property resulting from the morphological evolution of GNRs. More importantly, the LSPR peak-shift-based DNA dendritic nanostructured biosensor possesses three advantages in sensing and detecting target nucleic acids: (1) It is completely label- and wash-free, (2) it has an ultrahigh sensitivity and signal-to-noise ratio, and (3) it can be visualized without any instrumental aid, indicating its potential in the application of ultrasensitive bioanalyte assays and clinical diagnosis (Scheme 1).

EXPERIMENTAL SECTION

Thiolated Molecule (CYS, GSH, BSA)-Mediated Overgrowth of GNRs. GNRs were prepared by the previously reported seed-mediated growth approach.[34] The colorimetric assay of CYS (GSH or BSA) was conducted by using the following procedure: 1.0 mL of 40 mM hexadecyltrimethylammonium chloride (CTAC), 20 μL of 100 mM L-ascorbic acid (AA), 25 μL of 1.0 mM $HAuCl_4$, and different concentrations of CYS (GSH or BSA) were loaded into a 1.5 mL tube. Subsequently, 250 μL of 0.10 nM GNRs was added into the different concentrations of CYS (GSH or BSA)-

https://dx.doi.org/10.1021/acs.analchem.0c00321
Anal. Chem. 2020, 92, 7054−7061

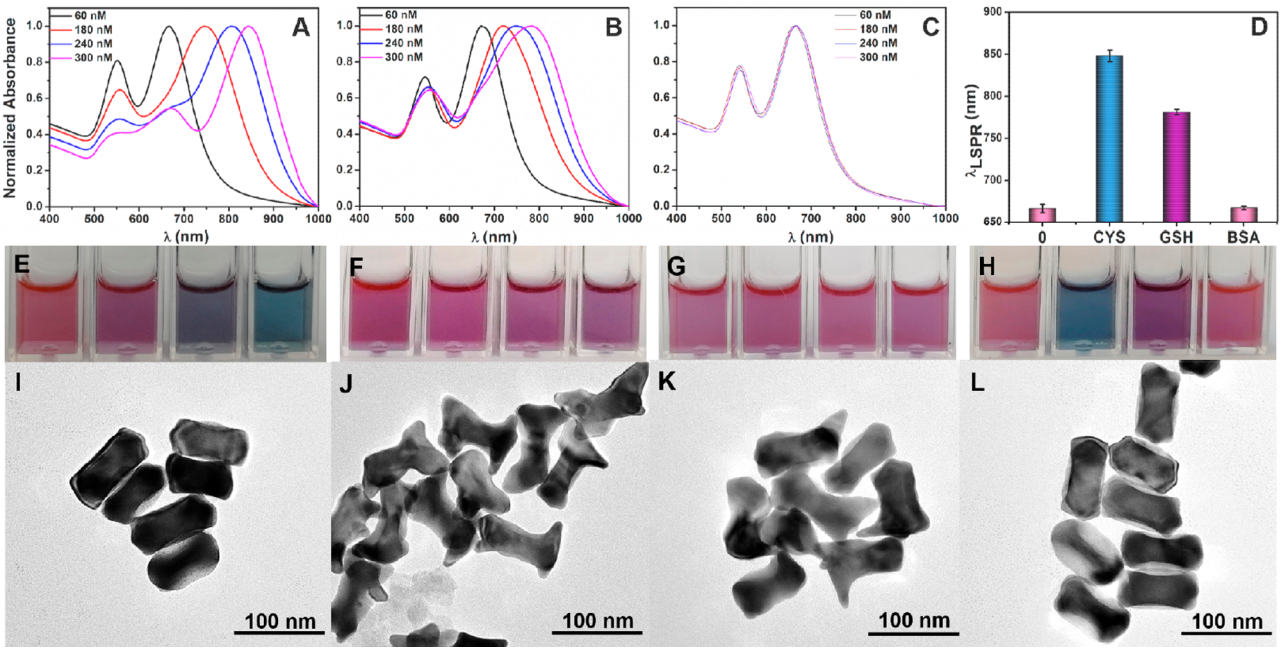

Figure 1. (A–C) Vis–NIR spectra and (E–G) corresponding photographs of the Au@gap@GNRs prepared at different concentrations of CYS, GSH, and BSA: 60, 180, 240, and 300 nM, respectively. (D) Plot of λ_{LSPR} and (H) corresponding photograph. (I–L) TEM images of the Au@gap@GNRs prepared at a 0 nM thiolated molecule and 300 nM of CYS, GSH, and BSA, respectively.

containing solution, and the mixture was gently shaken for several seconds to form solution 1. After incubation for 0.5 h at 25 °C, 25 μL of 10 mM $HAuCl_4$ was added to each tube to form solution 2. A color change was observed in seconds, and the tubes were incubated for another 0.5 h at 25 °C. The Au@gap@GNRs were washed twice at 5000 rpm for 20 min and finally stored in the same volume of water solution for transmission electron microscopy (TEM) characterization. The absorption spectra of the GNRs in the presence of different concentrations of CYS (GSH or BSA) were recorded.

Synthesis of DNA Dendrimers by Nonlinear Hybridization Chain Reaction. DNA dendrimers were prepared by the previously reported nonlinear hybridization chain reaction (HCR).[35] The sequences of the oligonucleotides are listed in Table S1. Experiments were performed in 1× TAE buffer (40 mM Tris, 20 mM HAc, 1 mM EDTA) supplemented with 12.5 mM Mg^{2+} (pH 8.0). Substrates A and B were separately prepared by heating the mixture of the substrate A (substrate B) strand and the substrate Ac (substrate Bc) strand to 95 °C for 5 min in a ratio of 1:1 and cooling to room temperature. The mixture of annealed substrates A and B was mixed with assistants A and B, respectively, and the resulting solutions were mixed with A (70 nM substrate A, 140 nM assistant A) and B (140 nM substrate B, 280 nM assistant B) in a ratio of 1:2. After the addition of certain amounts of target DNA, the tubes were incubated for 2 h at 30 °C. The next overgrowth process was the same as thiolated molecule-mediated growth of GNRs.

RESULTS AND DISCUSSION

Roles of Thiolated Biomolecules as Capping Agents in the Overgrowth of GNRs. In our previous work, we achieved the fine control of GNR overgrowth with tunable LSPR properties by adding different concentrations of thiolated peptides.[36] To fully explore the mechanism of the capping ligand size-dependent LSPR property, research was first conducted using the different sizes of thiolated amino acids, peptides, and proteins as classes of capping ligands in the overgrowth of GNRs. First, the synthetic GNRs displayed a light-brown color with LSPR absorptions at 700 nm and an average aspect ratio of 3.73 (length: 64.67 ± 5.83 nm; width: 17.33 ± 1.14 nm, Figure S1). As shown in Figure 1A,B,E,F, increasing the concentration of CYS and GSH resulted in the red shift of the LSPR peak and a colorimetric change from pink to purple and even to blue, which was detectable by the naked eye. An increase in the number of tips and the aspect ratio of the Au@gap@GNRs could also be observed (Figure S2, Table S2) because the thiolated biomolecules could readily replace CTAB at the ends of the GNRs (111) instead of the sides of the GNRs (100, 110). Furthermore, CTAB has a lower packing density on the (111) end face than on the (100) side face, and the exposed (111) end face of the GNR with high active sites has a preferential tendency to bind to thiolated molecules.[37] Subsequently, it is expected that the overgrowth of the GNRs from the GNR surface experienced an electrostatic interaction between the thiolated molecules and $AuCl_4^-$ after the thiolated molecules anchored onto the GNRs.[38] More TEM images were selected to prove that GSH preferentially binds to the ends of GNRs (Figure S3). The lattice fringes with distances of 0.235 nm in the high-resolution TEM images were assigned to the (111) Au crystalline planes (Figure S4). The scanning TEM and corresponding energy-dispersive spectroscopy (EDS) mapping revealed the presence of sulfur from GSH molecules on the surface of the GNRs after centrifugal purification (Figure S5). In fact, with the same concentration of capping agents (300 nM), larger-sized peptides experienced a greater blue shift of the LSPR peak than the amino acids in the overgrowth of the GNR (Figure 1D). Moreover, with 300 nM thiolated molecules, CYS could reach blue, whereas GSH could only reach purple in the overgrowth of GNRs because the steric hindrance of the thiolated molecules resulted in a decrease in the adsorption

https://dx.doi.org/10.1021/acs.analchem.0c00321
Anal. Chem. 2020, 92, 7054–7061

rate of the GSH molecules on the end of the GNRs (Figure 1H). However, the LSPR property and the color of the solution showed a negligible change with BSA (66 kDa) as a capping ligand because its inherent size is too large to be entrapped (Figure 1C,D,G,H). In addition, metallothioneins, a group of cysteine-rich proteins with a low molecular weight (6.5 kDa),[39] experience the same phenomenon as BSA, without any color change in the solution (Figure S6). In detail, the morphological evolution of Au@gap@GNRs prepared at a 0 nM thiolated molecule and at 300 nM of CYS, GSH, and BSA, respectively, is shown in Figure 1I–L. The corresponding LSPR peak, aspect ratio, and sizes of CYS, GSH, and BSA are shown in Table 1. The sizes of CYS and GSH were calculated (CYS: 0.9 nm × 0.6 nm × 0.5 nm; GSH: 1.8 nm × 0.9 nm × 0.7 nm, Figure S7), and the size of BSA was obtained from the literature (14 nm × 3.8 nm × 3.8 nm).[40] This shows that the size of the capping agent is also an important factor in regulating LSPR properties, in addition to the concentration of the capping agent. To verify the effectiveness of the thiol, thiol-free amino acids (such as glycine, lysine, arginine, and proline) were used for a similar overgrowth of the GNR (Figure S8). The results show that like the large-sized BSA and the absence of thiolated biomolecules, thiol-free amino acids as capping ligands have no obvious changes in the overgrowth of the GNR as well. This indicates that the thiol group is another important factor in regulating LSPR properties in addition to the concentration and size of the capping ligand.

Table 1. Characteristics of Au@gap@GNR Prepared at a 0 nM Thiolated Molecule and 300 nM of CYS, GSH, and BSA, Respectively

capping agent	R_0 of thiolated molecules (nm)[a]	λ_{LSPR} (nm)	aspect ratio
no thiolated molecule		668 ± 3	2.24
CYS	0.40	848 ± 3	2.61
GSH	0.65	780 ± 4	2.47
BSA	3.64	665 ± 3	2.22

[a] R_0: The radius of 3D thiolated biomolecules simulated as spheres.

In summary, different concentrations and sizes of thiolated biomolecules as capping ligands to control the overgrowth of GNRs are proposed herein, resulting in Au@gap@GNRs with tunable geometric and plasmonic properties. Detailed experimental studies showed three representative factors for the morphological control and LSPR properties using the thiolated biomolecules as capping ligands. One was influenced by the presence of thiol that promoted longitudinal growth due to selective binding to the ends of the GNRs, which increased their aspect ratio. The second was influenced by the concentration of the capping ligands that induced more reaction sites and tips at the ends of the GNRs, also leading to a further increase in the aspect ratio of the Au@gap@GNRs. The last factor was the size of the capping ligands, which could be divided into two situations: (1) When the capping ligands are small molecules (such as CYS, GSH), the gold shell growing behind could wrap small molecules. In other words, small molecules have been entrapped within the internal gap of Au@gap@GNR. Also, the LSPR peak is blue-shifted as the size of the capping ligand increases because the steric hindrance results in a decrease in the adsorption rate of the capping ligand on the GNRs. (2) When the capping ligands are macromolecular proteins (such as BSA, metallothioneins), the gold shell growing behind cannot wrap the proteins due to its large size. This results in a morphology and spectra similar to the Au@gap@GNRs without thiolated biomolecules as capping ligands. A combination of the above three factors can explain the mechanism of Au@gap@GNR with tunable morphologies and LSPR properties encoded by thiolated molecules.

Roles of Thiol-Free and Nonhomooligomeric DNA as Capping Ligands in Synthesizing Au@gap@GNRs. Among all known biomolecules as capping ligands, DNA, as an excellent material module, has a uniquely programmable and functional ability, following the highly specific Watson–Crick base-pairing rule. It can form various geometries and motifs and precisely assemble into different sizes of DNA nanostructures compared with amino acids, peptides, and

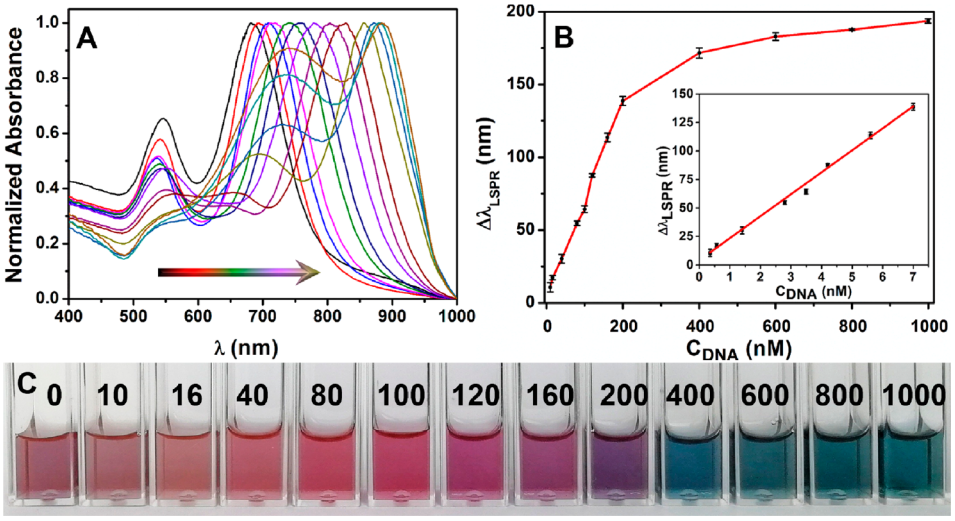

Figure 2. (A) Vis–NIR spectra and (C) corresponding photographs of the DNA-mediated Au@gap@GNRs prepared at different concentrations of DNA: 0, 10, 16, 40, 80, 100, 120, 160, 200, 400, 600, 800, and 1000 nM, respectively. (B) Red-shifted wavelength of the LSPR peak ($\Delta\lambda_{LSPR}$) of the DNA-mediated GNRs as a function of DNA concentration for the detection.

https://dx.doi.org/10.1021/acs.analchem.0c00321
Anal. Chem. 2020, 92, 7054–7061

proteins. In addition, DNA with a functional group can also be modified and adsorbed to the surface of noble nanoparticles. As a result, DNA, as a capping ligand, perfectly conforms to the above three factors in regulating the morphology and LSPR properties of Au@gap@GNR. Various research efforts have been conducted on the use of homooligomeric DNA as an engineered code for regulating the morphology in the overgrowth of mono- and bimetallic nanoparticles due to the different affinities of DNA bases to the surface of a GNR.[41,42] However, sequence-dependent systems hinder the widespread applications of DNA nanotechnology. Interestingly, we have shown that thiol-free and nonhomooligomeric DNA strands (random-DNA: ATCG ATCG ATCG) have a similar phenomenon as that of thiolated biomolecules in the concentration effect on the overgrowth of GNRs. Namely, as the concentration of capping ligands increases, a red shift of the LSPR peak and apparent colorimetric changes of the solutions ranging from pink to purple, and even to blue, can be observed (Figure 2). We have also found that a much lower concentration of DNA (120 nM) compared with CYS (200 nM) and GSH (300 nM) could lead to the same red shift (780 nm) of the LSPR peak of GNRs. This also proves that DNA strands have a stronger ability to shape the morphology of GNRs compared with thiolated molecules.

To further explain the role of thiol-free and nonhomooligomeric DNA strands in regulating the geometric properties of Au@gap@GNRs, TEM was used to image the resulting Au@gap@GNRs. We found that thiol-free DNA strands can also be selectively adsorbed to the ends of GNRs without modified functional groups in the DNA in the overgrowth of GNRs, accompanied by an increase in the aspect ratio (Figure 3, Table S3). DNA is in the gap between the gold shell formed later and GNRs as seeds. This is the origin of the tips on the ends of GNRs. To further investigate the impact of different DNA nucleobases on the formation of the Au@gap@GNRs, we conducted syntheses with oligo dA12 (A_{12}), oligo dT12 (T_{12}), oligo dC12 (C_{12}), and oligo dG12 (G_{12}). A_{12}, C_{12}, and G_{12} resulted in a red shift of the LSPR peak and a colorimetric change, except for T_{12}, in the overgrowth of the GNRs (Figure 4A–H). However, the TSPR peak changes of A_{12}, C_{12}, and G_{12} were different. This is because CTAB has a lower packing density on the (111) end face than on the (100) side face, and the exposed (111) end face of the GNR with highly active sites has a preferential tendency to bind to DNA molecules. Furthermore, the competitive adsorption experiments on the gold surface show that the relative adsorption affinity of the DNA nucleobases is A > C > G > T.[2,43] By increasing the A_{12} concentration, A_{12} could be adsorbed longitudinally as well as transversely because A has the strongest adsorption affinity (Figure 4A,I, Figure S9A–C). Therefore, the width of the GNRs was slightly increased by 5 nm, and the length increase (~15 nm) was more obvious in the A_{12}-mediated overgrowth of the GNR with the increase in A_{12} concentration (Table S4). Because G does not have a particularly strong adsorption affinity on the gold surface, it preferably bonds to the two ends of the GNR (Figure 4L, Figure S9J–L). As such, the adsorption affinity of C is between that of A and G, which results in the shape of the Au@gap@GNR with C_{12} as a capping agent between the shapes of the A_{12}- and G_{12}-mediated overgrowth of the GNR. Therefore, the TSPR peak of the C_{12}-mediated overgrowth of GNRs was broadened (by 100 nm) because a smaller part of C_{12} was adsorbed transversely on the GNR, resulting in an uneven transverse size (Figure 4C,K, Figure S9G–I). T_{12}, like BSA, did not result in any change, suggesting that the majority of the T_{12} did not adsorb to the surface of the GNR because the adsorption affinity on the gold surface was too weak (Figure 4B,J, Figure S9D–F). Therefore, the red shift of the LSPR peak depends on A, C, and G. In general, DNA nanotechnology involves these three bases almost exclusively. By taking advantage of the DNA strands as capping agents and the LSPR property from the morphological evolution of the GNR, the $\Delta\lambda_{LSPR}$-based biosensor exhibited promising detection and imaging results.

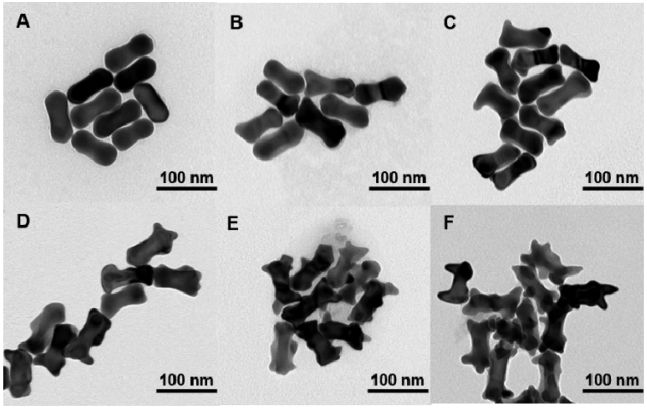

Figure 3. (A–F) TEM images of the DNA-mediated Au@gap@GNRs produced with 10, 80, 120, 200, 400, and 1000 nM random-DNA, respectively.

Application of Capping Ligand Size-Dependent LSPR Property. Taking advantage of the high predictability and the resulting spatial nanostructures, DNA nanotechnology has been rapidly expanded and enriched, facilitating the significant potential for applications including nanoscale devices as well as optical and plasmonic sensors. We have found that DNA nanostructures with varying spatial sizes as capping ligands can control the evolution of the geometric and plasmonic properties of the Au@gap@GNR. The $\Delta\lambda_{LSPR}$-based biosensor via DNA nanostructure-mediate GNR overgrowth has three representative advantages: (1) It is a label- and wash-free platform for the detection of target DNA, (2) the $\Delta\lambda_{LSPR}$-based biosensor has an ultrahigh sensitivity and signal-to-noise ratio, and (3) ultrasensitive visualization is possible without any instrumental aid. Therefore, we constructed a nonlinear HCR platform in which target DNA initiates the self-sustained assembly of double-stranded substrates into DNA dendritic nanostructures according to what was previously reported (Scheme 1B). Next, DNA dendrimers were used as capping agents to promote the overgrowth of the GNR. The mechanism of the $\Delta\lambda_{LSPR}$-based biosensor corresponded to the size effect of thiolated molecules in the overgrowth of the GNRs. As shown in Figure 5A–C, the resulting phenomenon is divided into two stages in the increase in the target DNA concentration: (1) DNA strands gradually assemble into DNA dendrimers, which leads to a reduction in the effective adsorption on the surface of the GNRs because the larger size of DNA dendrimers has more steric hindrance compared with DNA strands, resulting in a blue shift in the LSPR peak (807–760 nm), in which the color of the solution changes from blue to purple. (2) As the concentration of the target DNA further increases, the increased number of reaction sites leads to a decrease in the average molecular weight of the DNA

https://dx.doi.org/10.1021/acs.analchem.0c00321
Anal. Chem. 2020, 92, 7054–7061

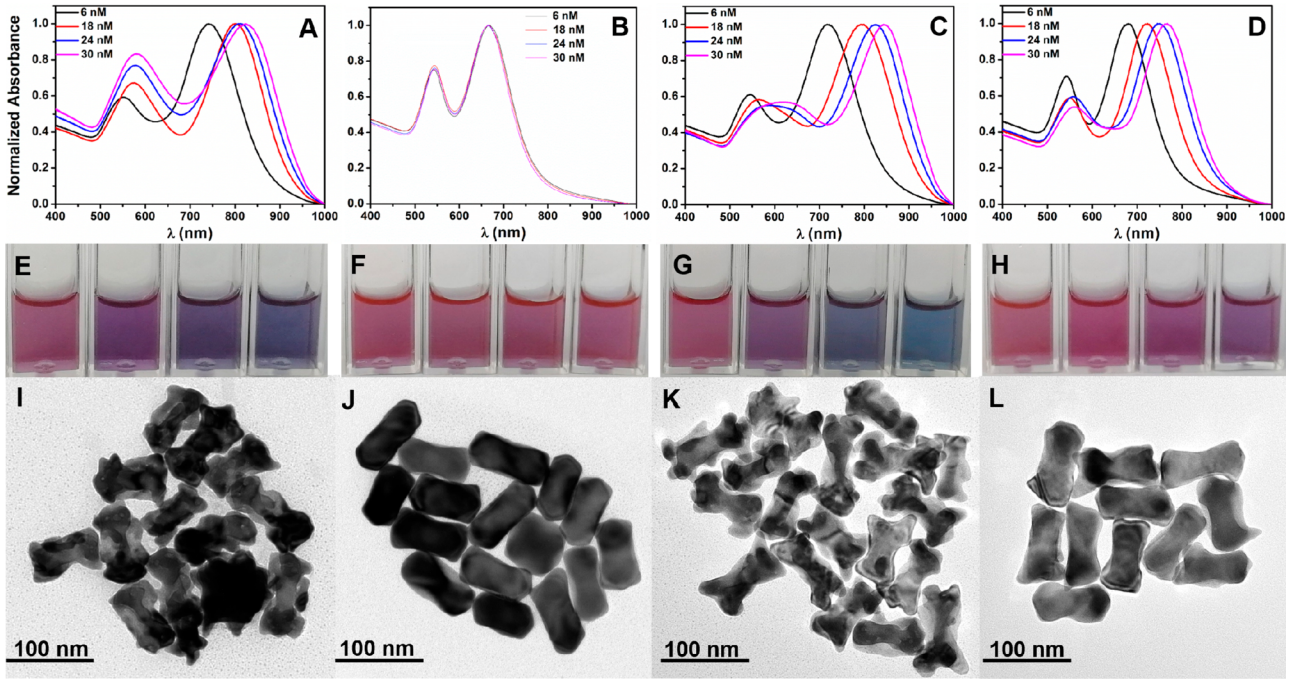

Figure 4. (A–D) Vis–NIR spectra and (E–H) corresponding photographs of the Au@gap@GNRs prepared at different concentrations of A_{12}, T_{12}, C_{12}, and G_{12}: 6, 18, 24, and 30 nM, respectively. (I–L) TEM images of the Au@gap@GNRs prepared at 30 nM of A_{12}, T_{12}, C_{12} and G_{12}, respectively.

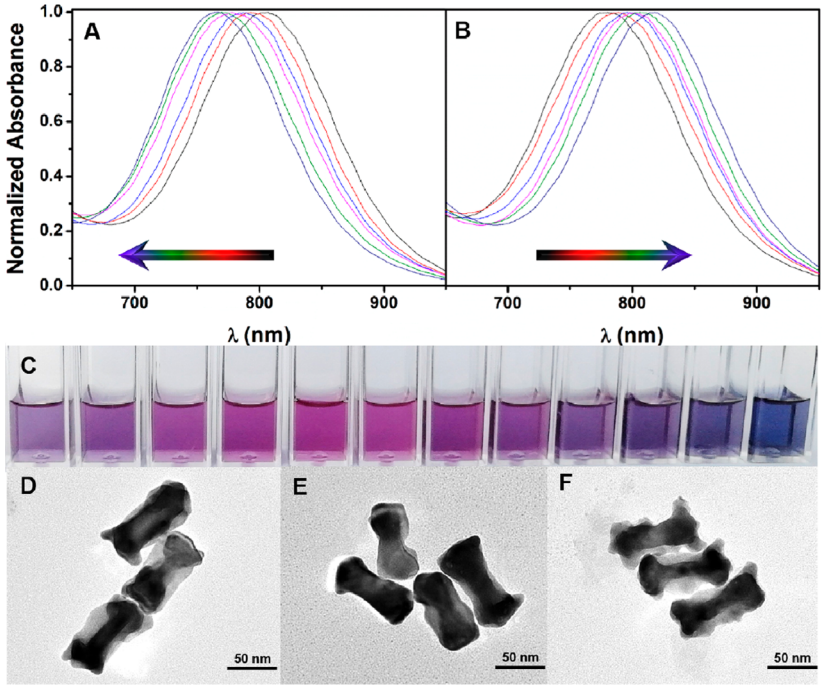

Figure 5. (A) Vis–NIR spectra of the DNA dendrimer-mediated Au@gap@GNRs prepared at different concentrations of target DNA: 0, 0.07, 0.14, 0.35, 0.42, and 0.56 nM, respectively. (B) Vis–NIR spectra of the DNA dendrimer-mediated Au@gap@GNRs prepared at different concentrations of target DNA: 0.7, 0.84, 1.05, 1.4, 2.8, and 3.5 nM, respectively. (C) Corresponding photographs of the DNA dendrimer-mediated Au@gap@GNRs prepared at different concentrations of DNA from 0 to 3.5 nM. (D–F) TEM images of the DNA dendrimer-mediated Au@gap@GNRs produced with 0.07, 0.56, and 3.5 nM target DNA, respectively.

nanostructure.[44] The smaller DNA nanostructures adsorbed to the ends of the GNR also increase, causing the LSPR peak to red shift (760–819 nm) and the color of the solution to change from purple to blue. Furthermore, native polyacrylamide gel electrophoresis (PAGE) also verified that the average molecular weight of the nonlinear HCR products varied inversely with the target DNA concentration (Figure S10). In addition, the TEM images indicated that in the resulting Au@gap@GNRs the aspect ratio becomes smaller (2.49–2.36) and then becomes larger (2.36–2.51, Figure 5D–F). Whereas the concentration of noncomplementary target DNA strands (Nc) increases, there is no two-stage change in the overgrowth of the

https://dx.doi.org/10.1021/acs.analchem.0c00321
Anal. Chem. 2020, 92, 7054–7061

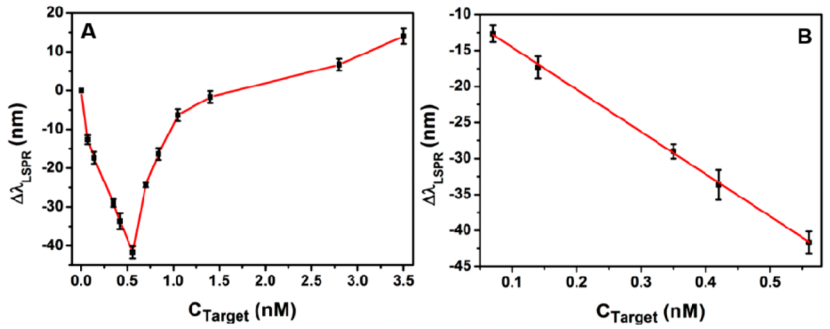

Figure 6. (A) Plot of $\Delta\lambda_{LSPR}$ of the DNA dendrimer-mediated Au@gap@GNRs as a function of the target DNA concentration. (B) Linear relationship of the $\Delta\lambda_{LSPR}$ versus the target DNA concentration.

GNR and the continuous red shift process of the LSPR peak, indicating that there is no generation of DNA nanostructures (Figure S11). The $\Delta\lambda_{LSPR}$-based biosensor used large dendritic nanostructures as capping agents with a detection limit of 19 pM (Figure 6). More importantly, the $\Delta\lambda_{LSPR}$-based biosensor was more convincing based on the size of the capping ligand compared with traditional and high-background-absorption peak-intensity-based colorimetric analyses and quenched group-based fluorescence analyses.

CONCLUSIONS

We have demonstrated the use of thiolated biomolecules with different concentrations and sizes to control the overgrowth of GNRs, resulting in nanoparticles with tunable geometric and plasmonic properties. The LSPR property, color, and morphological evolution of Au@gap@GNRs showed the size-dependent effect of the capping ligand. Interestingly, by increasing the concentration of thiol-free and nonhomooligomeric DNA strands, the red shift of the LSPR peak was similar to that using thiolated molecules as capping agents in GNR overgrowth. Studies with DNA strands as a capping agent revealed two representative pathways for the morphological evolution of GNRs. DNA molecules are excellent material modules for assembling nanostructures with different sizes and shapes. Therefore, we explored the mechanism and application of the DNA dendritic nanostructure as a capping agent combined with LSPR signals generated by the morphological evolution of Au@gap@GNR. More importantly, the $\Delta\lambda_{LSPR}$-based biosensor has an ultrahigh sensitivity and signal-to-noise ratio compared with traditional colorimetric and fluorescence analyses. Therefore, by taking advantage of DNA strands as capping agents and the LSPR property from the morphological evolution of GNRs, the $\Delta\lambda_{LSPR}$-based biosensor exhibits potential applications in biorecognition, sensing, and therapy.

ASSOCIATED CONTENT

Supporting Information

The Supporting Information is available free of charge at https://pubs.acs.org/doi/10.1021/acs.analchem.0c00321.

Detailed methodological description of the materials and reagents, apparatus, TEM images of GNRs and Au@gap@GNRs, EDS mapping of the GSH-mediated GNRs, the chemical structure and size of CYS and GSH, Vis−NIR spectra of metallothioneins and thiol-free amino-acid-mediated overgrowth of GNRs, native PAGE, selectivity of the $\Delta\lambda_{LSPR}$-based biosensor, sequences of DNA strands, and the aspect ratio of Au@gap@GNRs (PDF)

AUTHOR INFORMATION

Corresponding Authors

Yong-Liang Yu − *Research Center for Analytical Sciences, Department of Chemistry, College of Sciences, Northeastern University, Shenyang 110819, China;* orcid.org/0000-0001-9763-0954; Email: yuyl@mail.neu.edu.cn

Jian-Hua Wang − *Research Center for Analytical Sciences, Department of Chemistry, College of Sciences, Northeastern University, Shenyang 110819, China;* orcid.org/0000-0003-2175-3610; Phone: +86 24 83688944; Email: jianhuajrz@mail.neu.edu.cn; Fax: +86 24 83676698

Authors

Meng-Qi He − *Research Center for Analytical Sciences, Department of Chemistry, College of Sciences, Northeastern University, Shenyang 110819, China*

Shuai Chen − *College of Life and Health Sciences, Northeastern University, Shenyang 110169, China*

Jie Meng − *Research Center for Analytical Sciences, Department of Chemistry, College of Sciences, Northeastern University, Shenyang 110819, China*

Wei Shi − *Research Center for Analytical Sciences, Department of Chemistry, College of Sciences, Northeastern University, Shenyang 110819, China*

Kun Wang − *Research Center for Analytical Sciences, Department of Chemistry, College of Sciences, Northeastern University, Shenyang 110819, China*

Complete contact information is available at: https://pubs.acs.org/10.1021/acs.analchem.0c00321

Notes

The authors declare no competing financial interest.

ACKNOWLEDGMENTS

This work is financially supported by the National Natural Science Foundation of China (21922402, 21874017, and 21727811), the Liaoning Provincial Program for Promoting Talents (XLYC1807005 and XLYC1802016), and the Fundamental Research Funds for the Central Universities (N180504003).

REFERENCES

(1) He, X.; Zhao, Z.; Xiong, L.-H.; Gao, P. F.; Peng, C.; Li, R. S.; Xiong, Y.; Li, Z.; Sung, H. H. Y.; Williams, I. D.; Kwok, R. T. K.; Lam, J. W. Y.; Huang, C. Z.; Ma, N.; Tang, B. Z. *J. Am. Chem. Soc.* **2018**, *140*, 6904−6911.

(2) Tan, L. H.; Yue, Y.; Satyavolu, N. S. R.; Ali, A. S.; Wang, Z.; Wu, Y.; Lu, Y. *J. Am. Chem. Soc.* **2015**, *137*, 14456−14464.

(3) Tan, L. H.; Xing, H.; Lu, Y. *Acc. Chem. Res.* **2014**, *47*, 1881−1890.
(4) Chen, K.; Lin, C.-C.; Vela, J.; Fang, N. *Anal. Chem.* **2015**, *87*, 4096−4099.
(5) Gu, Y.; Song, J.; Li, M.-X.; Zhang, T.-T.; Zhao, W.; Xu, J.-J.; Liu, M.; Chen, H.-Y. *Anal. Chem.* **2017**, *89*, 10585−10591.
(6) Hou, H.; Wang, P.; Zhang, J.; Li, C.; Jin, Y. *ACS Appl. Mater. Interfaces* **2015**, *7*, 18038−18045.
(7) Shen, J.; Liang, L.; Xiao, M.; Xie, X.; Wang, F.; Li, Q.; Ge, Z.; Li, J.; Shi, J.; Wang, L.; Li, L.; Pei, H.; Fan, C. *J. Am. Chem. Soc.* **2019**, *141*, 11938−11946.
(8) Oh, J.-W.; Lim, D.-K.; Kim, G.-H.; Suh, Y. D.; Nam, J.-M. *J. Am. Chem. Soc.* **2014**, *136*, 14052−14059.
(9) Jiang, R.; Li, B.; Fang, C.; Wang, J. *Adv. Mater.* **2014**, *26*, 5274−5309.
(10) Lu, J.; Chang, Y.-X.; Zhang, N.-N.; Wei, Y.; Li, A.-J.; Tai, J.; Xue, Y.; Wang, Z.-Y.; Yang, Y.; Zhao, L.; Lu, Z.-Y.; Liu, K. *ACS Nano* **2017**, *11*, 3463−3475.
(11) Kou, X.; Zhang, S.; Yang, Z.; Tsung, C.-K.; Stucky, G. D.; Sun, L.; Wang, J.; Yan, C. *J. Am. Chem. Soc.* **2007**, *129*, 6402−6404.
(12) Sun, Z.; Ni, W.; Yang, Z.; Kou, X.; Li, L.; Wang, J. *Small* **2008**, *4*, 1287−1292.
(13) Dickerson, M. B.; Sandhage, K. H.; Naik, R. R. *Chem. Rev.* **2008**, *108*, 4935−4978.
(14) Palafox-Hernandez, J. P.; Lim, C.-K.; Tang, Z.; Drew, K. L. M.; Hughes, Z. E.; Li, Y.; Swihart, M. T.; Prasad, P. N.; Knecht, M. R.; Walsh, T. R. *ACS Appl. Mater. Interfaces* **2016**, *8*, 1050−1060.
(15) Zhao, B.; Shen, J.; Chen, S.; Wang, D.; Li, F.; Mathur, S.; Song, S.; Fan, C. *Chem. Sci.* **2014**, *5*, 4460−4466.
(16) Wang, Z.; Tang, L.; Tan, L. H.; Li, J.; Lu, Y. *Angew. Chem., Int. Ed.* **2012**, *51*, 9078−9082.
(17) He, M.-Q.; Wang, K.; Wang, W.-J.; Yu, Y.-L.; Wang, J.-H. *Anal. Chem.* **2017**, *89*, 9292−9298.
(18) Li, D.; Zhou, W.; Yuan, R.; Xiang, Y. *Anal. Chem.* **2017**, *89*, 9934−9940.
(19) Tang, Y.; Lin, Y.; Yang, X.; Wang, Z.; Le, X. C.; Li, F. *Anal. Chem.* **2015**, *87*, 8063−8066.
(20) Liu, L.; Liu, J.-W.; Wu, H.; Wang, X.-N.; Yu, R.-Q.; Jiang, J.-H. *Anal. Chem.* **2018**, *90*, 1502−1505.
(21) Song, T.; Tang, L.; Tan, L. H.; Wang, X.; Satyavolu, N. S. R.; Xing, H.; Wang, Z.; Li, J.; Liang, H.; Lu, Y. *Angew. Chem., Int. Ed.* **2015**, *54*, 8114−8118.
(22) Pinheiro, A. V.; Han, D.; Shih, W. M.; Yan, H. *Nat. Nanotechnol.* **2011**, *6*, 763−772.
(23) Huang, J.; Wu, Y.; Chen, Y.; Zhu, Z.; Yang, X.; Yang, C. J.; Wang, K.; Tan, W. *Angew. Chem., Int. Ed.* **2011**, *50*, 401−404.
(24) Zeng, Y.; Pei, J.-J.; Wang, L.-H.; Shen, A.-G.; Hu, J.-M. *Biosens. Bioelectron.* **2015**, *66*, 55−61.
(25) He, H.; Dai, J.; Duan, Z.; Meng, Y.; Zhou, C.; Long, Y.; Zheng, B.; Du, J.; Guo, Y.; Xiao, D. *Biosens. Bioelectron.* **2016**, *86*, 985−989.
(26) Liu, S.; Cheng, C.; Liu, T.; Wang, L.; Gong, H.; Li, F. *Biosens. Bioelectron.* **2015**, *63*, 99−104.
(27) Zhang, X.; Cheng, R.; Shi, Z.; Jin, Y. *Biosens. Bioelectron.* **2016**, *75*, 101−107.
(28) He, H.; Xu, X.; Wu, H.; Jin, Y. *Adv. Mater.* **2012**, *24*, 1736−1740.
(29) Fang, W.-F.; Chen, W.-J.; Yang, J.-T. *Sens. Actuators, B* **2014**, *192*, 77−82.
(30) Wang, J.; Zhang, P.; Li, C. M.; Li, Y. F.; Huang, C. Z. *Biosens. Bioelectron.* **2012**, *34*, 197−201.
(31) He, M. Q.; Chen, S.; Yao, K.; Wang, K.; Yu, Y. L.; Wang, J. H. *Small Methods* **2019**, *3*, 1900017.
(32) Liu, J.; Wang, S.; Cai, K.; Li, Y.; Liu, Z.; Liu, L.; Han, Y.; Wang, H.; Han, H.; Chen, H. *Small* **2019**, *15*, 1900444.
(33) Xia, Y.; Gilroy, K. D.; Peng, H.-C.; Xia, X. *Angew. Chem., Int. Ed.* **2017**, *56*, 60−95.
(34) Zheng, G.; Bao, Z.; Perez-Juste, J.; Du, R.; Liu, W.; Dai, J.; Zhang, W.; Lee, L. Y. S.; Wong, K.-Y. *Angew. Chem., Int. Ed.* **2018**, *57*, 16452−16457.
(35) Xuan, F.; Hsing, I. M. *J. Am. Chem. Soc.* **2014**, *136*, 9810−9813.
(36) He, M.-Q.; Chen, S.; Yao, K.; Meng, J.; Wang, K.; Yu, Y.-L.; Wang, J.-H. *Anal. Chem.* **2020**, *92*, 1395−1401.
(37) Chang, J.-Y.; Wu, H.; Chen, H.; Ling, Y.-C.; Tan, W. *Chem. Commun.* **2005**, 1092−1094.
(38) Ma, X.; Huh, J.; Park, W.; Lee, L. P.; Kwon, Y. J.; Sim, S. J. *Nat. Commun.* **2016**, *7*, 12873.
(39) Margoshes, M.; Vallee, B. L. *J. Am. Chem. Soc.* **1957**, *79*, 4813−4814.
(40) Song, Y.; Fan, J.-B.; Li, X.; Liang, X.; Wang, S. *Adv. Mater.* **2019**, *31*, 1900391.
(41) Satyavolu, N. S. R.; Tan, L. H.; Lu, Y. *J. Am. Chem. Soc.* **2016**, *138*, 16542−16548.
(42) Quintanilla, M.; Kuttner, C.; Smith, J. D.; Seifert, A.; Skrabalak, S. E.; Liz-Marzán, L. M. *Nanoscale* **2019**, *11*, 19561−19570.
(43) Satyavolu, N. S. R.; Loh, K. Y.; Tan, L. H.; Lu, Y. *Small* **2019**, *15*, 1900975.
(44) Dirks, R. M.; Pierce, N. A. *Proc. Natl. Acad. Sci. U. S. A.* **2004**, *101*, 15275−15278.

https://dx.doi.org/10.1021/acs.analchem.0c00321
Anal. Chem. 2020, 92, 7054−7061